HHS Public Access

Author manuscript

Brain Struct Funct. Author manuscript; available in PMC 2022 November 10.

Published in final edited form as:

Brain Struct Funct. 2022 July ; 227(6): 2111–2125. doi:10.1007/s00429-022-02503-z.

Aging and white matter microstructure and macrostructure: a longitudinal multi-site diffusion MRI study of 1218 participants

Kurt G. Schilling[1], **Derek Archer**[2,3,4], **Fang-Cheng Yeh**[6,11], **Francois Rheault**[7], **Leon Y. Cai**[7], **Colin Hansen**[7], **Qi Yang**[7], **Karthik Ramdass**[7], **Andrea T. Shafer**[8], **Susan M. Resnick**[8], **Kimberly R. Pechman**[2,3], **Katherine A. Gifford**[2,3], **Timothy J. Hohman**[2,3,4], **Angela Jefferson**[2,3,5], **Adam W. Anderson**[9], **Hakmook Kang**[10], **Bennett A. Landman**[7]

[1]Department of Radiology and Radiological Sciences, Vanderbilt University Medical Center, Nashville, TN, USA

[2]Vanderbilt Memory and Alzheimer's Center, Vanderbilt University Medical Center, Nashville, TN, USA

[3]Department of Neurology, Vanderbilt University Medical Center, Nashville, TN, USA

[4]Vanderbilt Genetics Institute, Vanderbilt University School of Medicine, Nashville, TN, USA

[5]Department of Medicine, Vanderbilt University Medical Center, Nashville, TN, USA

[6]Department of Neurological Surgery, University of Pittsburgh Medical Center, Pittsburgh, PA, USA

[7]Department of Electrical Engineering and Computer Science, Vanderbilt University, Nashville, TN, USA

[8]Laboratory of Behavioral Neuroscience, National Institute on Aging, National Institutes of Health, Baltimore, MD, USA

[9]Department of Biomedical Engineering, Vanderbilt University, Nashville, TN, USA

[10]Department of Biostatistics, Vanderbilt University, Nashville, TN, USA

[11]Department of Bioengineering, University of Pittsburgh, Pittsburgh, PA, USA

Abstract

✉ Kurt G. Schilling kurt.g.schilling.1@vumc.org.

Author contributions All authors contributed to the study conception and design. Data collection was performed by the Baltimore Longitudinal Study of Aging at the National Institutes of Aging, and the Vanderbilt Memory & Aging Project (VMAP). All authors commented on previous versions of the manuscript. All authors read and approved the final manuscript.

Declarations

Conflict of interest The authors have no relevant financial or non-financial interests to disclose.

Ethical approval All human data sets from Vanderbilt University were acquired after informed consent under supervision of the appropriate Institutional Review Board. All additional data sets are freely available and unrestricted for non-commercial research purposes. This study accessed only de-identified patient information.

Consent to participate Informed consent was obtained from all individual participants included in the study.

Supplementary Information The online version contains supplementary material available at https://doi.org/10.1007/s00429-022-02503-z.

Quantifying the microstructural and macrostructural geometrical features of the human brain's connections is necessary for understanding normal aging and disease. Here, we examine brain white matter diffusion magnetic resonance imaging data from one cross-sectional and two longitudinal data sets totaling in 1218 subjects and 2459 sessions of people aged 50–97 years. Data was drawn from well-established cohorts, including the Baltimore Longitudinal Study of Aging data set, Cambridge Centre for Ageing Neuroscience data set, and the Vanderbilt Memory & Aging Project. Quantifying 4 microstructural features and, for the first time, 11 macrostructure-based features of volume, area, and length across 120 white matter pathways, we apply linear mixed effect modeling to investigate changes in pathway-specific features over time, and document large age associations within white matter. Conventional diffusion tensor microstructure indices are the most age-sensitive measures, with positive age associations for diffusivities and negative age associations with anisotropies, with similar patterns observed across all pathways. Similarly, pathway shape measures also change with age, with negative age associations for most length, surface area, and volume-based features. A particularly novel finding of this study is that while trends were homogeneous throughout the brain for microstructure features, macrostructural features demonstrated heterogeneity across pathways, whereby several projection, thalamic, and commissural tracts exhibited more decline with age compared to association and limbic tracts. The findings from this large-scale study provide a comprehensive overview of the age-related decline in white matter and demonstrate that macrostructural features may be more sensitive to heterogeneous white matter decline. Therefore, leveraging macrostructural features may be useful for studying aging and could facilitate comparisons in a variety of diseases or abnormal conditions.

Keywords

White matter; Aging; Tractography; Volume; Diffusion MRI

Introduction

To better understand changes related to normal aging, and differences due to disease, it is necessary to characterize how and where the brain changes with age. Studies using magnetic resonance imaging (MRI) have shown that the brain undergoes significant changes with age. Most studies focus on gray matter of the brain, where correlations between cortical volumes and age have been consistently described. These findings provide evidence of heterogenous patterns of normal age-related changes (Ramanoel et al. 2018; Terribilli et al. 2011; Bergfield et al. 2010; Taki et al. 2011; Giorgio et al. 2010; Zuo et al. 2021), with detectable differences in neurological diseases and disorders (Pfefferbaum et al. 1992; Kimmel et al. 2016; Wang et al. 2019; Jorge et al. 2021; Guo et al. 2014).

While white matter appears relatively homogenous on conventional structural MRI, diffusion MRI and subsequent fiber tractography enables investigation of individual fiber pathways of the brain. To date, most diffusion MRI studies of aging characterize features of tissue microstructure using cross-sectional data sets. For example, diffusion tensor imaging (DTI) shows fractional anisotropy (FA) is negatively associated with age, and mean diffusivity (MD) positively associated with age across white matter pathways (Abe

et al. 2008; Storsve et al. 2016; Yap et al. 2013; Lebel et al. 2012), and have shown that advanced multicompartment diffusion modeling also provides sensitive measures of age-related microstructural changes (Beck et al. 2021; Toschi et al. 2020; Chang et al. 2015; Cox et al. 2016), including measures of neurite volume fractions and dispersion (Beck et al. 2021; Lawrence et al. 2021), diffusion restrictions (Lawrence et al. 2021), axon diameters (Fan et al. 2019), and measures of non-Gaussianity (Dong et al. 2020; Coutu et al. 2014). Microstructural features of these fiber pathways are biologically relevant in aging research as demyelination is thought to occur in a heterogeneous manner, whereby late-myelinating fiber pathways exhibit neurodegeneration prior to other fiber pathways. This idea, known as the myelodegeneration hypothesis, has recently been supported by a large-scale diffusion MRI study leveraging data from the UK Biobank (n = 7167) (Isaac Tseng et al. 2021). Specifically, they found disproportional age-related differences in fiber pathways projecting to/from the prefrontal cortex.

While diffusion-based microstructure has been widely studied in aging, the macrostructural features of these fiber pathways play a pivotal role along the aging continuum; however, they have yet to be studied. As recently described (Yeh 2020), these macrostructural properties —descriptions of lengths, areas, and volumes—can be used to describe the geometrical and connectivity features of fiber bundles. The incorporation of these features into the study of aging and aging-related disorders could provide an additional avenue to elucidate the mechanisms driving white matter neurodegeneration. Given our prior knowledge, our hypothesis is that microstructural and macrostructural features will be disproportionately affected in fiber tracts projecting to/from the prefrontal cortex along the aging continuum.

To address our hypothesis, we will leverage three well-established cohorts of aging, including two longitudinal cohorts [Baltimore Longitudinal Study of Aging (BLSA) (Williams et al. 2019), Vanderbilt Memory & Aging Project (VMAP) (Jefferson et al. 2016)] and one cross-sectional cohort [Cambridge Centre for Ageing and Neuroscience (Cam-CAN) (Taylor et al. 2017)]. Within these cohorts, automated state-of-the art tractography segmentation will be conducted within 120 white matter tracts, including association, limbic, projection (including thalamic and striatal), and commissural tracts. We will then quantify 11 macrostructural features within these tracts, and 4 previously described microstructural features, to determine if these metrics exhibit disproportionate age-related decline.

Methods

Data

This study used data from three data sets, summarized in Table 1, and contained a total of 1218 subjects and 2459 sessions of healthy subjects aged 50–97 years. All data sets were filtered to exclude subjects with diagnoses of mild cognitive impairment, Alzheimer's disease, or dementia at baseline, or if they developed these conditions during the follow-up interval. Finally, data sets were filtered to focus on subjects aged 50+, due to limited samples sizes of each data set with subjects below 50 years.

First, was the Baltimore Longitudinal Study of Aging (BLSA) data set, with 675 subjects scanned multiple times ranging from 1 and 8 sessions, and time between scans ranging from 1 to 10 years, yielding a total of 1545 diffusion data sets. Diffusion MRI data was acquired on a 3 T Philips Achieva scanner (32 gradient directions, b value = 700 s/mm^2, TR/TE = 7454/75 ms, reconstructed voxel size = 0.81 × 0.81 × 2.2 mm, reconstruction matrix = 320 × 320, acquisition matrix = 115 × 115, field of view = 260 × 260 mm). Second, was data from the Vanderbilt Memory & Aging Project (VMAP), with 187 subjects, scanned between 1 and 4 sessions, with a total of 558 diffusion data sets. Diffusion MRI data was acquired on a 3 T Philips Achieva scanner (32 gradient directions, b value = 1000 s/mm^2, reconstructed voxel size = 2 × 2 × 2 mm). Third, was data from the Cambridge Centre for Ageing and Neuroscience (Cam-CAN) data repository (Taylor et al. 2017) with 356 subjects, each scanned once using a 3 T Siemens TIM Trio scanner with a 32-channel head coil (30 directions at b value = 1000 s/mm^2, 30 directions at b value = 2000s/mm^2, reconstructed voxel size = 2 × 2 × 2 mm). All human data sets from Vanderbilt University were acquired after informed consent under supervision of the appropriate Institutional Review Board. All additional data sets are freely available and unrestricted for non-commercial research purposes. This study accessed only de-identified patient information.

Processing

For every session, sets of white matter pathways were virtually dissected using two automated fiber tractography pipelines, TractSeg (Wasserthal et al. 2018) and Automatic Track Recognition (ATR) (Yeh et al. 2018). Two methods, based on different technological and anatomical principles of tractography segmentation were selected to emphasize generalizability of results across choices of different workflow (Schilling et al. 2021a).

Throughout the manuscript, TractSeg analysis is presented as primary results, and ATR as supplementary.

Briefly, TractSeg was based on convolutional neural networks and performed bundle-specific tractography based on a field of estimated fiber orientations (Wasserthal et al. 2018). We implemented the dockerized version at (https://github.com/MIC-DKFZ/TractSeg), which generated fiber orientations using constrained spherical deconvolution with the MRtrix3 software (Tournier et al. 2019). TractSeg resulted in 71 bundles, visualized in Fig. 1, including association, limbic, commissural, thalamic, striatal, and projection and cerebellar pathways.

ATR was performed in DSI Studio software using batch automated fiber tracking (Yeh et al. 2018). Data were reconstructed using generalized q-sampling imaging (Yeh et al. 2010) with a diffusion sampling length ratio of 1.25. A deterministic fiber tracking algorithm (Yeh et al. 2013) was used in combination with anatomical priors from a tractography atlas (Yeh et al. 2018) to map all pathways using inclusion and exclusion regions of interest. Topology-informed pruning (Yeh et al. 2019) was applied to the tractography with 16 iterations to remove false connections. The Dockerized source code is available at http://dsi-studio.labsolver.org. ATR resulted. In 49 bundles, visualized in. Supplementary Fig. 1, including association, limbic, commissural, thalamic, and projection pathways.

For each session, and every pathway, several features were extracted. Four microstructural features included DTI metrics of FA, MD, radial diffusivity (RD), and axial diffusivity (AD). The 11 macrostructure-based features extracted from each pathway (details described in (Yeh 2020)) are based on length (mean length, span, diameter; units of mm), area (total surface area, total area of end regions; units of mm^2), volume (total volume, trunk volume, branch volume; units of mm^3), and shape (curl, elongation, irregularity; unitless). Summary descriptions and equations for all macrostructural features are shown in Table 2.

Quality control (QC) was performed to minimize possible false results due to acquisition issues or failure of tractography. For acquisition related QC, sessions were removed from analysis if the diffusion weighted correlation was less than 3 standard deviations away from the mean correlation (for each data set), or if signal slice dropout occurred in > 10% of slices (~3 slices). Individual bundles were removed from the analysis if the number of segmented streamlines was less than 3 standard deviations away from the mean number (for each pathway), or if the total number of streamlines was below 200 (indicating failure of tractography), and subjects were removed from analysis if > 20% of pathways failed QC. We note that this stringent QC still resulted in $N > 1700$ samples for all but 9 pathways. The total number of samples per data set is given in supplementary data (Supplementary Table 1 and Supplementary Table 2), and a list of abbreviations for all 120 (71 + 49) pathways is given in the “Appendix”.

Analytical plan

To investigate the relationship between age and each WM feature, linear mixed effects modeling was performed, with each (z-normalized) feature, Y, modeled as a linear function of age, $y = \beta_0 + \beta_1 Age + \beta_2 Sex + \beta_3 TICV + \beta_4 CSFV + \beta_5(1 + AGE|DATASET) + \beta_6(SUB)$,, where subjects (SUB) were entered as a random effect (i.e., subject-specific random intercept), and subject sex (Sex), total intracranial volume (TICV), and CSF volume (CSFV) as fixed effects. In addition, we modelled the association between age and outcome variable as data set (DATASET) specific due to expected differences in MR protocols (Jones and Diffusion 2010; Farrell et al. 2007; Landman et al. 2007; Schilling et al. 2021c; Ning et al. 2020), and included a data set specific random slope and intercept. We note that the TICV utilized was calculated from the T1-weighted image from the baseline scan, and is scaled appropriately depending on units of the feature, Y (scaled by TICV/4pi)^(1/2) for area, and scaled by (3*TICV/4pi)^(1/3 for length).

Due to multiple comparisons, all statistical tests were controlled by the false discovery rate at 0.05 to determine significance. All results are presented as the beta coefficient of estimate ‘B_1’, or in other words “the association of the feature ‘y’ with Age”, which (due to normalization) represents the standard deviation change in feature per year. These measures are derived for each pathway and each feature. Supplementary results additionally show the results as a percent change per year, derived from the slope normalized by the average value across the aging population (from 50 to 97), and multiplied by 100, which represents the percent change in feature per year.

Results

Total intracranial volume, white matter, gray matter, and CSF

Supplementary Fig. 2 shows results of global changes in tissue volume. Total GM and WM tissue volumes decrease, along with increases in CSF volumes, in agreement with the literature. While GM, CSF, and global tissue volume are not the primary aims of this study, we did find significant age associations with these measures.

What changes and where?

To summarize association with age for all features and all pathways, we show the beta coefficient associations with age for all features in matrix form in Fig. 2, along with boxplots highlighting the percent change for all microstructure and all macrostructure features. Similar results, but shown as the percent-change-per-year from linear mixed effects models, are shown in Supplementary Fig. 3.

Most notably, microstructure measures show fairly homogenous changes across all pathways, with negative associations for FA, and again positive associations for diffusivities, with median association coefficients with age of − 0.02, and approximately + 0.02 to + 0.03, respectively (changes of − 0.2% per year, and +0.3–0.5% per year, respectively). In general, features of length, area, and volumes decrease with age, however, changes are heterogenous across pathways. Measures of volume (total volume, trunk volume, branch volume) show median associations across pathways of − 0.4, − 0.4, and − 0.4 (changes of − 0.9%, − 0.9%, and − 0.6% per year). Elongation show positive trends with age, while irregularity decreases with age.

Large commissural pathways (the body, splenium, and genu of the corpus callosum), as well as thalamic and striatal projections show the strongest negative trends of all features of size with age. In addition, a number of association fibers and fasciculi, including the SLF sub-components, ILF, FAT, MLF, and PAT of both hemispheres show trends with age for all shape features, with greater changes in volumes and area of end regions than mean lengths and spans.

Supplementary Figs. 4 and 5 show results from the ATR fiber tractography (for fit coefficients and percent-change per year, respectively), which indicate similar changes with age and in similar locations, with fit coefficients and percent-change per year of similar magnitudes. FA shows negative associations with age, diffusivities show positive associations, with microstructure measures associations similar across all pathways. Measures of volume show the greatest negative associations with age, with larger changes in the commissural and thalamic pathways.

Visualizing change

To visualize where these changes occur, Fig. 3 shows example streamlines, separated into association, limbic, commissural, thalamic, projection, and striatal pathways, with bundles colored using the previous colormaps, and only showing bundles with statistically significant changes (Fig. 3 shows the Beta coefficients from linear mixed-effects models,

Supplementary Fig. 6 shows results interpreted as percent-change per year). Notably, the changes in FA and MD are similar, with the corticospinal tract (CST) changing the least (yet still statistically significant) with age, and the forceps major and anterior thalamic and striatal radiations, which occupy a majority of frontal lobe white matter space, changing the most. Other pathways show relatively homogenous change across age. Volumes and End Region Areas show similar trends, with large changes in the frontal lobe pathways, large changes in white matter of the occipital lobe, and small (but statistically significant) changes in the pathways associated with motor and pre-motor regions. The mean length decreases at a much smaller rate per year, remaining statistically significant, with visual exceptions of AC (a small commissural pathway), and projection pathways (including striatal and thalamic) to the occipital lobe. Similarly, the left and right OR show increased length with age, which would be an intuitive result of increased CSF (i.e., larger ventricles), and thus a more tortuous path from occipital lobe to thalamus. Similar results, in similar locations, are confirmed using pathways segmented using ATR, and are shown in Supplementary Fig. 7 (as Beta coefficients) and Supplementary Fig. 8 (as percent-change per year).

Pathways of interest

To provide even more insight into the microstructural and macrostructural associations shown in this study, we have provided illustrations for a projection tract (i.e., anterior thalamic radiation, Fig. 4) and commissural tract (i.e., forceps minor, Fig. 5). For the anterior thalamic radiation (3D illustration in Fig. 4A), we found significant age-related decline in all four microstructural measures (Fig. 4B), in which there was a positive age-related association with MD (p = 3E-5), RD (p = 5E-5), and AD (p = 6E-4), and a negative association with FA (p = 3E-4). There were also several significant associations with macrostructural features for this tract. Figure 4C illustrates 4 of these associations, including volume (p = 1E-6), branch volume (p = 3E-3), surface area (p = 1E-7), and area of end regions (p = 0.02). Figure 5 illustrates the associations for the forceps minor tract, again demonstrating significant positive age-related associations with diffusivities, negative age-related associations with FA, and negative age-related associations with volume, surface area, and area of end regions.

As expected, plots of the microstructure features and LME best-fit lines in Figs. 4 and 5 show considerable differences between data sets (Ning et al. 2020; Fortin et al. 2017; Mirzaalian et al. 2016). While less described in the literature (Schilling et al. 2021c), scanner effects are also introduced in the tractography macrostructural analysis, typically leading to data set-specific *intercepts*, however, with similar age-related *slopes*. These trends generalize to all pathways, for both microstructural and macrostructural features (see “Discussion”), justify the use of random effects in the LME model, and emphasize the generalizability of age-related trends across all data sets.

Discussion

Using a large, cross sectional and longitudinal data set, we analyze microstructural features and, for the first time, shape-based features, of WM pathways across age. We found that while microstructural features were globally sensitive to age-related decline, these measures

were largely homogeneous in their decline across the association, limbic, projection, thalamic, striatal, and commissural fibers. In contrast, we found that macrostructural features were non-uniform in their trends in age-related decline. In general, we found that, the thalamic and striatal fibers demonstrated the most age-related decline, followed the projection and commissural fibers, and finally association and limbic fibers. Thus, macrostructural features may be more specific in identifying age-related WM decline and could a more sensitive marker for neurodegenerative disorders compared to microstructural features.

Age-related microstructural decline

Trends seen in diffusion microstructure indices mirror that from existing literature (Lebel et al. 2012; Beck et al. 2021; Lawrence et al. 2021; Fan et al. 2019; Bigham et al. 2022; Ardekani et al. 2007; Lebel et al. 2008), which we have confirmed generalize to larger data sets, and across data sets with different scanners, vendors, and acquisitions. Diffusivities increase with age, with the largest change shown for radial, and mean diffusivities, and to a lesser extent, axial diffusivities. Consequently, this leads to a decrease in fractional anisotropy. This has traditionally been attributed to myelin loss and/or decreased axonal volume fractions and densities (Lebel et al. 2012; Cox et al. 2016; Lebel et al. 2008; Groot et al. 2015; Molloy et al. 2021; Nicolas et al. 2020), with supplemental evidence provided through advanced multicompartment modeling (Beck et al. 2021; Cox et al. 2016). However, care must be taken when interpreting these indices as highly specific markers of tissue microstructure, as diffusion (and DTI in particular) is sensitive to a number of potential biophysical changes (Wheeler-Kingshott and Cercignani 2009).

Towards this end, a wealth of microstructural models and diffusion representations have emerged in recent years, enabling quantitative measures of neurite densities (Lawrence et al. 2021), intra- and extra-cellular diffusivities (Beck et al. 2021; Lawrence et al. 2021), axonal dispersion (Lawrence et al. 2021), axon diameters (Fan et al. 2019), and diffusion non-Gaussianity (Lawrence et al. 2021; Dong et al. 2020), among others, which have been shown to be sensitive to age-related changes in white matter. While DTI is generally most sensitive to age-related changes throughout the entire white matter (Lawrence et al. 2021), these other measures may not only be more specific to microstructure but may offer improved sensitivity within specific pathways. Here, 2 of our data sets (VMAP, BLSA) are single shell acquisitions and do not offer the ability to perform advanced modeling, but there is potential to further explore microstructural measures using other data sets, for example HCP-aging or UK-Biobank, that incorporate multiple diffusion weightings, in combination with the macrostructural features proven here.

As expected, the data sets used in this study showed large effects on quantified measures (Ning et al. 2020; Tax et al. 2019) due to differences in acquisition conditions (Farrell et al. 2007; Landman et al. 2007; Jones and Basser 2004), although the same trends were seen across data sets, with only small differences in associations with age. Combination of data sets in analysis requires either accounting for these effects in modeling (as performed here) or harmonizing data across scanners and sites, which is an active area of interest (Ning et

al. 2020; Fortin et al. 2017; Mirzaalian et al. 2016). Harmonization studies can utilize these well-characterized effects of age as validation of techniques and algorithms.

Age-related macrostructural decline

While tractography has been used to study the human brain in aging, it is often used to simply extract pathway-specific indices of microstructure (or quantitative) measures. Here, we study shape-based features of tractography-defined bundles, quantifying basic features (e.g., length, diameter, volume) and more comprehensive features (e.g., curl, irregularity, elongation). We find that, indeed, the shape of white matter features changes with age. Notably, basic macrostructural features such as volume and total surface areas exhibit age-related decline, in agreement with the observed trend of a decrease in total white matter volume. Furthermore, more comprehensive measures, such as irregularity and elongation, show age-related changes such as an increased length-to-diameter ratio (elongation) that capture how the overall geometry is changing. While both length and diameter decrease, the space occupied by the pathway decreases at a faster rate. Length is constrained to connect one cortical region to another and is limited in how fast it can decrease while maintaining a connection, and in some cases may even increase to account for ventricular expansion. In contrast, axonal loss or overall white matter volume loss leads to the faster decreasing bundle diameter.

In our subsequent analysis to determine if there was heterogeneous age-related decline between the association, limbic, association, striatal, thalamic, and commissural tracts, we found widespread significant differences (see Fig. 2). For example, striatal and thalamic pathways generally show the largest age-related changes in volumes, surface areas, diameters, and even microstructure, followed by commissural, and finally projection, limbic, and association pathways (although even within these sub-types we find heterogenous changes). Age-related changes in dimensionless elongation (length ÷ diameter) or irregularity [surface area ÷ (π × diameter × length)] were relatively low in the association and limbic tracts but higher in projection, commissural, thalamic, and striatal pathways.

Our findings, therefore, indicate that specific white matter features can be used to identify age-related decline, and these features can also be incorporated into clinical populations to identify abnormal aging patterns. Future work should investigate different trends in disease cohorts, where this analysis facilitates asking “what changes?” and “where?”. This also results in the creation of a large feature space (10’s of pathways × 10’s of features) for each subject, which may facilitate machine learning, deep learning, and dimensionality reduction techniques to identify abnormalities in an individual subject or cohort. Similar analysis may also be used in an unsupervised fashion—rather than utilizing predefined bundles, a connectome-style approach can be used to extract every fiber bundle in a large connectome matrix followed by subsequent feature-based analysis of every edge in the connectome.

Like microstructure features, differences in data sets led to very different quantitative shape properties which are known to be affected by scanners, vendors, resolution, and acquisition settings (Schilling et al. 2021b; Rheault et al. 2020; Chamberland et al. 2018). In particular, the CAM–CAM shows the largest differences, likely due to the use of a multi-shell acquisition, and its effects on local reconstruction algorithms (Schilling et al. 2018; Daducci

et al. 2014; Fillard et al. 2011). The random effects of data set were most pronounced on the estimated feature intercepts, rather than slope, thus similar age-related trends are observed for all data sets, and generalize to all acquisitions. Future studies should utilize additional fiber tractography bundle segmentation algorithms, (Wasserthal et al. 2018; Winter et al. 2021; Warrington et al. 2020; Guevara et al. 2012; Yendiki et al. 2011), based on different features of the signal and streamlines, which may include additional fiber pathways or may be more robust to data acquisition.

Global and local changes

In general, all pathways show consistent changes in tissue microstructure with age, indicating a largely global change in microstructure. In contrast, shape features of pathways show very different effect sizes and relative changes per year across the brain, which indicates local changes, and pathway-specific differences image. Overall, this suggests that microstructure features of pathways change together, and at relatively the same rates, whereas macrostructural features do not and indicate location-specific indices of change, whereby projection and commissural fibers exhibit more significant age-related decline. Thus, pathway features might be a more sensitive biomarker for differences due to disease or disorders.

It is possible to further refine localization specificity of the DTI based analysis using an along tract analysis, or along-fiber quantification (AFQ). Assigning microstructural indices to positions along a pathway enables analysis of age-related changes at certain positions within this pathway. While the novelty of this work is the study of multiple shape and geometrical macrostructural features of white matter across age, we did perform an AFQ analysis of our 4 microstructural features using a bundle analytics framework with LME modeling (Chandio et al. 2020), and show exemplar results for different pathway types in Fig. 6 (with AFQ of all pathways given is Supplementary Figs. 9–14). In general, microstructural changes are relatively consistent across an entire pathway, with notable exceptions in the CST (at the mid-brain) and callosal pathways (at the center-line). This nicely parallels the macrostructural analysis, with generally similar declines in volume in both the trunk and branches of the pathways. Future work should investigate specific locations within pathways that are sensitive to age-related changes, but also investigate possible AFQ-style analysis for shape-based features, for example along-pathway diameters or volumes.

Limitations

This study has several limitations. While we utilized large samples sizes and showed generalizability to very different aging data sets, results were tested on just one bundle segmentation algorithm. In addition, many pathways were investigated, significantly more than is typical for many studies on aging, and many of these pathways are smaller association pathways that may be harder or more variable to track. Nevertheless, the large sample size facilitated statistical analysis and findings with small effect sizes. The use of different data sets with different acquisitions is known to result in very different quantitative indices, and in the current study, very different tractography results. However, we consider

this an advantage to the current study, where results generalized across all data, and effect of data set was included in modeling.

Future studies should investigate and characterize shape changes across the lifespan. This may be particularly relevant in childhood, where large changes in brain structure and microstructure are expected. Second, the combination of shape and microstructure features in disease should be investigated. There is a significant body of research on DTI changes in disease, and it is intuitive that the shape, location, and geometry of pathways may also experience significant alterations in such states. Finally, the relationship between GM regions and WM structure should be investigated. The full feature space of GM volume, thickness, and surface area, in combination with WM macrostructure and microstructure features, will facilitate a complete description of changes in the brain during aging.

Conclusions

We provide a comprehensive characterization of WM changes in aging. Using large cross-sectional and longitudinal diffusion data sets, we have shown that both microstructural and macrostructural geometrical features of the human brain change during normal aging. Microstructural indices of anisotropy and diffusivity show the largest effects with age, with global trends apparent across all pathways. Macrostructural features of volume, surfaces areas, and lengths also change with age, with trends that are not uniform across all pathways. Thus, tract-specific changes in geometry occur in normal aging. Results from this study may be useful in understanding biophysical and structural changes occurring during normal aging and will facilitate comparisons in a variety of diseases or abnormal conditions.

Supplementary Material

Refer to Web version on PubMed Central for supplementary material.

Funding

This work was supported by the National Science Foundation Career Award #1452485, the National Institutes of Health under award numbers R01EB017230, K01AG073584, and in part by ViSE/VICTR VR3029 and the National Center for Research Resources, Grant UL1 RR024975–01.

Data availability

Derived microstructure and macrostructure features, for all pathways and subjects, along with demographic information, are made available at (link upon acceptance) for the CAMCAN data set. Data from VMAP are available by request at http://vmacdata.org/vmap/data-requests. Data from the BLSA are available on request from the BLSA website (http://blsa.nih.gov). All requests are reviewed by the BLSA Data Sharing Proposal Review Committee and may also be subject to approval from the NIH institutional review board.

Appendix

The bundles resulting from each segmentation pipeline are given as a list below, with acronyms used in the text.

TractSeg: Arcuate fascicle left (AF_L); Arcuate fascicle right (AF_R); Anterior Thalamic Radiation left (ATR_L); Thalamic Radiation right; (ATR_R); Commissure Anterior (CA); Rostrum (CC_1; Genu (CC_2); Rostral body (Premotor) (CC_3); Anterior midbody (Primary Motor) (CC_4); Posterior midbody (Primary Somatosensory) (CC_5); Isthmus (CC_6); Splenium (CC_7); Corpus Callosum—all (CC); Cingulum left (CG_L); Cingulum right (CG_R); Corticospinal tract left (CST_L); Corticospinal tract right (CST_R); Fronto-pontine tract left (FPT_L); Fronto-pontine tract right (FPT_R); Fornix left (FX_L); Fornix right (FX_R); Inferior cerebellar peduncle left (ICP_L); Inferior cerebellar peduncle right (ICP_R); Inferior occipito-frontal fascicle left (IFO_L); Inferior occipito-frontal fascicle right (IFO_R); Inferior longitudinal fascicle left (ILF_L); Inferior longitudinal fascicle right (ILF_R); Middle cerebellar peduncle (MCP); Middle longitudinal fascicle left (MLF_L); Middle longitudinal fascicle right (MLF_R); Optic radiation left (OR_L); Optic radiation right (OR_R); Parieto-occipital pontine left (POPT_L); Parieto-occipital pontine right (POPT_R); Superior cerebellar peduncle left (SCP_L); Superior cerebellar peduncle right (SCP_R); Superior longitudinal fascicle III left SLF_III_L); Superior longitudinal fascicle III right (SLF_III_R); Superior longitudinal fascicle II left (SLF_II_L); Superior longitudinal fascicle II right (SLF_II_R); Superior longitudinal fascicle I left (SLF_I_L); Superior longitudinal fascicle I right (SLF_I_R); Striato-fronto-orbital left (ST_FO_L); Striato-fronto-orbital right (ST_FO_R); Striato-occipital left (ST_OCC_L); Striato-occipital right (ST_OCC_R); Striato-parietal left (ST_PAR_L); Striato-parietal right (ST_PAR_R); Striato-postcentral left (ST_POSTC_L); Striato-postcentral right (ST_POSTC_R); Striato-precentral left (ST_PREC_L); Striato-precentral right (ST_PREC_R); Striato-prefrontal left (ST_PREF_L); Striato-prefrontal right (ST_PREF_R); Striato-premotor left (ST_PREM_L); Striato-premotor right (ST_PREM_R); Thalamo-occipital left (T_OCC_L); Thalamo-occipital right (T_OCC_R); Thalamo-parietal left (T_PAR_L); Thalamo-parietal right (T_PAR_R); Thalamo-postcentral left (T_POSTC_L); Thalamo-postcentral right (T_POSTC_R); Thalamo-precentral left (T_PREC_L); Thalamo-precentral right (T_PREC_R); Thalamo-prefrontal left (T_PREF_L); Thalamo-prefrontal right (T_PREF_R); Thalamo-premotor left (T_PREM_L); Thalamo-premotor right (T_PREM_R); Uncinate fascicle left (UF_L); Uncinate fascicle right (UF_R).

ATR: Arcuate_Fasciculus_L (AF_L); Arcuate Fasciculus R (AF_R); Cortico Spinal Tract L (CST_L); Cortico Spinal Tract R (CST_R); Cortico Striatal Pathway L (CS_L); Cortico Striatal Pathway R (CS_R); Corticobulbar Tract L (CBT_L); Corticobulbar Tract R (CBT_R); Corticopontine Tract L (CPT_L); Corticopontine Tract R (CPT_R); Corticothalamic Pathway L (CTP_L); Corticothalamic Pathway R (CTP_R); Inferior Cerebellar Peduncle L (ICP_L); Inferior Cerebellar Peduncle R (ICP_R); Inferior Fronto Occipital Fasciculus L (IFOF_L); Inferior Fronto Occipital Fasciculus R (IFOF_R); Inferior Longitudinal Fasciculus L (ILF_L); Inferior Longitudinal Fasciculus R (ILF_R); Optic Radiation L (OR_L); Optic Radiation R (OR_R); Middle Longitudinal Fasciculus L (MdLF_L); Middle Longitudinal Fasciculus R (MdLF_R); Uncinate Fasciculus L (UF_L); Uncinate Fasciculus R (UF_R).

References

Abe O, Yamasue H, Aoki S et al. (2008) Aging in the CNS: comparison of gray/white matter volume and diffusion tensor data. Neurobiol Aging 29(1):102–116. 10.1016/j.neurobiolaging.2006.09.003 [PubMed: 17023094]

Ardekani S, Kumar A, Bartzokis G, Sinha U (2007) Exploratory voxel-based analysis of diffusion indices and hemispheric asymmetry in normal aging. Magn Reson Imaging 25(2):154–167. 10.1016/j.mri.2006.09.045 [PubMed: 17275609]

Beck D, de Lange AG, Maximov II et al. (2021) White matter microstructure across the adult lifespan: a mixed longitudinal and cross-sectional study using advanced diffusion models and brain-age prediction. Neuroimage 224:117441. 10.1016/j.neuroimage.2020.117441 [PubMed: 33039618]

Bergfield KL, Hanson KD, Chen K et al. (2010) Age-related networks of regional covariance in MRI gray matter: reproducible multivariate patterns in healthy aging. Neuroimage 49(2):1750–1759. 10.1016/j.neuroimage.2009.09.051 [PubMed: 19796692]

Bigham B, Zamanpour SA, Zare H (2022) Alzheimer's disease neuroimaging I. Features of the superficial white matter as biomarkers for the detection of Alzheimer's disease and mild cognitive impairment: a diffusion tensor imaging study. Heliyon 8(1):08725. 10.1016/j.heliyon.2022.e08725

Chamberland M, Tax CMW, Jones DK (2018) Meyer's loop tractography for image-guided surgery depends on imaging protocol and hardware. Neuroimage Clin 20:458–465. 10.1016/j.nicl.2018.08.021 [PubMed: 30128284]

Chandio BQ, Risacher SL, Pestilli F et al. (2020) Bundle analytics, a computational framework for investigating the shapes and profiles of brain pathways across populations. Sci Rep 10(1):17149. 10.1038/s41598-020-74054-4 [PubMed: 33051471]

Chang YS, Owen JP, Pojman NJ et al. (2015) White matter changes of neurite density and fiber orientation dispersion during human brain maturation. PLoS One 10(6):e0123656. 10.1371/journal.pone.0123656 [PubMed: 26115451]

Coutu JP, Chen JJ, Rosas HD, Salat DH (2014) Non-Gaussian water diffusion in aging white matter. Neurobiol Aging 35(6):1412–1421. 10.1016/j.neurobiolaging.2013.12.001 [PubMed: 24378085]

Cox SR, Ritchie SJ, Tucker-Drob EM et al. (2016) Ageing and brain white matter structure in 3513 UK Biobank participants. Nat Commun 7:13629. 10.1038/ncomms13629 [PubMed: 27976682]

Daducci A, Canales-Rodríguez EJ, Descoteaux M et al. (2014) Quantitative comparison of reconstruction methods for intra-voxel fiber recovery from diffusion MRI. IEEE Trans Med Imaging 33(2):384–399. 10.1109/TMI.2013.2285500 [PubMed: 24132007]

de Groot M, Ikram MA, Akoudad S et al. (2015) Tract-specific white matter degeneration in aging: the Rotterdam study. Alzheimers Dement 11(3):321–330. 10.1016/jjalz.2014.06.011 [PubMed: 25217294]

Dong JW, Jelescu IO, Ades-Aron B et al. (2020) Diffusion MRI biomarkers of white matter microstructure vary nonmonotonically with increasing cerebral amyloid deposition. Neurobiol Aging 89:118–128. 10.1016/j.neurobiolaging.2020.01.009 [PubMed: 32111392]

Fan Q, Tian Q, Ohringer NA et al. (2019) Age-related alterations in axonal microstructure in the corpus callosum measured by high-gradient diffusion MRI. Neuroimage 191:325–336. 10.1016/j.neuroimage.2019.02.036 [PubMed: 30790671]

Farrell JA, Landman BA, Jones CK et al. (2007) Effects of signal-to-noise ratio on the accuracy and reproducibility of diffusion tensor imaging-derived fractional anisotropy, mean diffusivity, and principal eigenvector measurements at 1.5 T. J Magn Reson Imaging 26(3):756–67. 10.1002/jmri.21053 [PubMed: 17729339]

Fillard P, Descoteaux M, Goh A et al. (2011) Quantitative evaluation of 10 tractography algorithms on a realistic diffusion MR phantom. Neuroimage 56(1):220–234. 10.1016/j.neuroimage.2011.01.032 [PubMed: 21256221]

Fortin JP, Parker D, Tunç B et al. (2017) Harmonization of multi-site diffusion tensor imaging data. Neuroimage 11(161):149–170. 10.1016/j.neuroimage.2017.08.047

Giorgio A, Santelli L, Tomassini V et al. (2010) Age-related changes in grey and white matter structure throughout adulthood. Neuroimage 51(3):943–951. 10.1016/j.neuroimage.2010.03.004 [PubMed: 20211265]

Guevara P, Duclap D, Poupon C et al. (2012) Automatic fiber bundle segmentation in massive tractography datasets using a multi-subject bundle atlas. Neuroimage 61(4):1083–1099. 10.1016/j.neuroimage.2012.02.071 [PubMed: 22414992]

Guo Y, Zhang Z, Zhou B et al. (2014) Grey-matter volume as a potential feature for the classification of Alzheimer's disease and mild cognitive impairment: an exploratory study. Neurosci Bull 30(3):477–489. 10.1007/s12264-013-1432-x [PubMed: 24760581]

Isaac Tseng WY, Hsu YC, Chen CL et al. (2021) Microstructural differences in white matter tracts across middle to late adulthood: a diffusion MRI study on 7167 UK Biobank participants. Neurobiol Aging 98:160–172. 10.1016/j.neurobiolaging.2020.10.006 [PubMed: 33290993]

Jefferson AL, Gifford KA, Acosta LM et al. (2016) The Vanderbilt memory & aging project: study design and baseline cohort overview. J Alzheimers Dis 52(2):539–559. 10.3233/JAD-150914 [PubMed: 26967211]

Jones DK (2010) Diffusion MRI: theory, methods, and application. Oxford University Press, Oxford, p 767

Jones DK, Basser PJ (2004) "Squashing peanuts and smashing pumpkins": how noise distorts diffusion-weighted MR data. Magn Reson Med 52(5):979–993. 10.1002/mrm.20283 [PubMed: 15508154]

Jorge L, Martins R, Canario N et al. (2021) Investigating the spatial associations between amyloid-beta deposition, grey matter volume, and neuroinflammation in Alzheimer's disease. J Alzheimers Dis 80(1):113–132. 10.3233/JAD-200840 [PubMed: 33523050]

Kimmel CL, Alhassoon OM, Wollman SC et al. (2016) Age-related parieto-occipital and other gray matter changes in borderline personality disorder: a meta-analysis of cortical and subcortical structures. Psychiatry Res Neuroimaging 251:15–25. 10.1016/j.pscychresns.2016.04.005 [PubMed: 27107250]

Landman BA, Farrell JA, Jones CK, Smith SA, Prince JL, Mori S (2007) Effects of diffusion weighting schemes on the reproducibility of DTI-derived fractional anisotropy, mean diffusivity, and principal eigenvector measurements at 1.5T. Neuroimage 36(4):1123–38. 10.1016/j.neuroimage.2007.02.056 [PubMed: 17532649]

Lawrence KE, Nabulsi L, Santhalingam V et al. (2021) Age and sex effects on advanced white matter microstructure measures in 15,628 older adults: a UK biobank study. Brain Imaging Behav 15(6):2813–2823. 10.1007/s11682-021-00548-y [PubMed: 34537917]

Lebel C, Walker L, Leemans A, Phillips L, Beaulieu C (2008) Microstructural maturation of the human brain from childhood to adulthood. Neuroimage 40(3):1044–1055. 10.1016/j.neuroimage.2007.12.053 [PubMed: 18295509]

Lebel C, Gee M, Camicioli R, Wieler M, Martin W, Beaulieu C (2012) Diffusion tensor imaging of white matter tract evolution over the lifespan. Neuroimage 60(1):340–352. 10.1016/j.neuroimage.2011.11.094 [PubMed: 22178809]

Mirzaalian H, Ning L, Savadjiev P et al. (2016) Inter-site and inter-scanner diffusion MRI data harmonization. Neuroimage 07(135):311–323. 10.1016/j.neuroimage.2016.04.041

Molloy CJ, Nugent S, Bokde ALW (2021) Alterations in diffusion measures of white matter integrity associated with healthy aging. J Gerontol A Biol Sci Med Sci 76(6):945–954. 10.1093/gerona/glz289 [PubMed: 31830253]

Nicolas R, Hiba B, Dilharreguy B et al. (2020) Changes over time of diffusion MRI in the white matter of aging brain, a good predictor of verbal recall. Front Aging Neurosci 12:218. 10.3389/fnagi.2020.00218 [PubMed: 32922282]

Ning L, Bonet-Carne E, Grussu F et al. (2020) Cross-scanner and cross-protocol multi-shell diffusion MRI data harmonization: algorithms and results. Neuroimage 221:117128. 10.1016/j.neuroimage.2020.117128 [PubMed: 32673745]

Pfefferbaum A, Lim KO, Zipursky RB et al. (1992) Brain gray and white matter volume loss accelerates with aging in chronic alcoholics: a quantitative MRI study. Alcohol Clin Exp Res 16(6):1078–1089. 10.1111/j.1530-0277.1992.tb00702.x [PubMed: 1471762]

Ramanoel S, Hoyau E, Kauffmann L et al. (2018) Gray matter volume and cognitive performance during normal aging. A Voxel-based morphometry study. Front Aging Neurosci 10:235. 10.3389/fnagi.2018.00235 [PubMed: 30123123]

Rheault F, De Benedictis A, Daducci A et al. (2020) Tractostorm: the what, why, and how of tractography dissection reproducibility. Hum Brain Mapp 41(7):1859–1874. 10.1002/hbm.24917 [PubMed: 31925871]

Schilling KG, Janve V, Gao Y, Stepniewska I, Landman BA, Anderson AW (2018) Histological validation of diffusion MRI fiber orientation distributions and dispersion. Neuroimage 01(165):200–221. 10.1016/j.neuroimage.2017.10.046

Schilling KG, Rheault F, Petit L et al. (2021a) Tractography dissection variability: what happens when 42 groups dissect 14 white matter bundles on the same dataset? Neuroimage 243:118502. 10.1016/j.neuroimage.2021.118502 [PubMed: 34433094]

Schilling KG, Tax CMW, Rheault F et al. (2021b) Fiber tractography bundle segmentation depends on scanner effects, acquisition, diffusion sensitization, and bundle segmentation workflow. bioRxiv. 10.1101/2021.03.17.435872

Schilling KG, Tax CMW, Rheault F et al. (2021c) Fiber tractography bundle segmentation depends on scanner effects, vendor effects, acquisition resolution, diffusion sampling scheme, diffusion sensitization, and bundle segmentation workflow. Neuroimage 242:118451. 10.1016/j.neuroimage.2021.118451 [PubMed: 34358660]

Storsve AB, Fjell AM, Yendiki A, Walhovd KB (2016) Longitudinal changes in white matter tract integrity across the adult lifespan and its relation to cortical thinning. PLoS One 11(6):e0156770. 10.1371/journal.pone.0156770 [PubMed: 27253393]

Taki Y, Thyreau B, Kinomura S et al. (2011) Correlations among brain gray matter volumes, age, gender, and hemisphere in healthy individuals. PLoS One 6(7):e22734. 10.1371/journal.pone.0022734 [PubMed: 21818377]

Tax CM, Grussu F, Kaden E et al. (2019) Cross-scanner and cross-protocol diffusion MRI data harmonisation: a benchmark database and evaluation of algorithms. Neuroimage. 10.1016/j.neuroimage.2019.01.077

Taylor JR, Williams N, Cusack R et al. (2017) The Cambridge Centre for Ageing and Neuroscience (Cam-CAN) data repository: structural and functional MRI, MEG, and cognitive data from a cross-sectional adult lifespan sample. Neuroimage 144(Pt B):262–269. 10.1016/j.neuroimage.2015.09.018 [PubMed: 26375206]

Terribilli D, Schaufelberger MS, Duran FL et al. (2011) Age-related gray matter volume changes in the brain during non-elderly adulthood. Neurobiol Aging 32(2):354–368. 10.1016/j.neurobiolaging.2009.02.008 [PubMed: 19282066]

Toschi N, Gisbert RA, Passamonti L, Canals S, De Santis S (2020) Multishell diffusion imaging reveals sex-specific trajectories of early white matter degeneration in normal aging. Neurobiol Aging 02(86):191–200. 10.1016/j.neurobiolaging.2019.11.014

Tournier JD, Smith R, Raffelt D et al. (2019) MRtrix3: a fast, flexible and open software framework for medical image processing and visualisation. Neuroimage 202:116137. 10.1016/j.neuroimage.2019.116137 [PubMed: 31473352]

Wang J, Knol MJ, Tiulpin A et al. (2019) Gray matter age prediction as a biomarker for risk of dementia. Proc Natl Acad Sci USA 116(42):21213–21218. 10.1073/pnas.1902376116 [PubMed: 31575746]

Warrington S, Bryant KL, Khrapitchev AA et al. (2020) XTRACT—standardised protocols for automated tractography in the human and macaque brain. Neuroimage 217:116923. 10.1016/j.neuroimage.2020.116923 [PubMed: 32407993]

Wasserthal J, Neher P, Maier-Hein KH (2018) TractSeg—fast and accurate white matter tract segmentation. Neuroimage 183:239–253. 10.1016/j.neuroimage.2018.07.070 [PubMed: 30086412]

Wheeler-Kingshott CA, Cercignani M (2009) About, “axial” and “radial” diffusivities. Magn Reson Med 61(5):1255–1260. 10.1002/mrm.21965 [PubMed: 19253405]

Williams OA, An Y, Beason-Held L et al. (2019) Vascular burden and APOE epsilon4 are associated with white matter microstructural decline in cognitively normal older adults. Neuroimage 188:572–583. 10.1016/j.neuroimage.2018.12.009 [PubMed: 30557663]

Winter M, Tallantyre EC, Brice TAW, Robertson NP, Jones DK, Chamberland M (2021) Tract-specific MRI measures explain learning and recall differences in multiple sclerosis. Brain Commun. 10.1093/braincomms/fcab065

Yap QJ, Teh I, Fusar-Poli P, Sum MY, Kuswanto C, Sim K (2013) Tracking cerebral white matter changes across the lifespan: insights from diffusion tensor imaging studies. J Neural Transm (Vienna) 120(9):1369–1395. 10.1007/s00702-013-0971-7 [PubMed: 23328950]

Yeh F-C (2020) Shape analysis of the human association pathways. bioRxiv. 10.1101/2020.04.19.049544

Yeh FC, Wedeen VJ, Tseng WY (2010) Generalized q-sampling imaging. IEEE Trans Med Imaging 29(9):1626–1635. 10.1109/TMI.2010.2045126 [PubMed: 20304721]

Yeh FC, Verstynen TD, Wang Y, Fernandez-Miranda JC, Tseng WY (2013) Deterministic diffusion fiber tracking improved by quantitative anisotropy. PLoS One 8(11):e80713. 10.1371/journal.pone.0080713 [PubMed: 24348913]

Yeh FC, Panesar S, Fernandes D et al. (2018) Population-averaged atlas of the macroscale human structural connectome and its network topology. Neuroimage 178:57–68. 10.1016/j.neuroimage.2018.05.027 [PubMed: 29758339]

Yeh FC, Panesar S, Barrios J et al. (2019) Automatic removal of false connections in diffusion MRI tractography using topology-informed pruning (TIP). Neurotherapeutics 16(1):52–58. 10.1007/s13311-018-0663-y [PubMed: 30218214]

Yendiki A, Panneck P, Srinivasan P et al. (2011) Automated probabilistic reconstruction of white-matter pathways in health and disease using an atlas of the underlying anatomy. Front Neuroinform 5:23. 10.3389/fninf.2011.00023 [PubMed: 22016733]

Zuo N, Hu T, Liu H, Sui J, Liu Y, Jiang T (2021) Gray matter-based age prediction characterizes different regional patterns. Neurosci Bull 37(1):94–98. 10.1007/s12264-020-00558-8 [PubMed: 32813179]

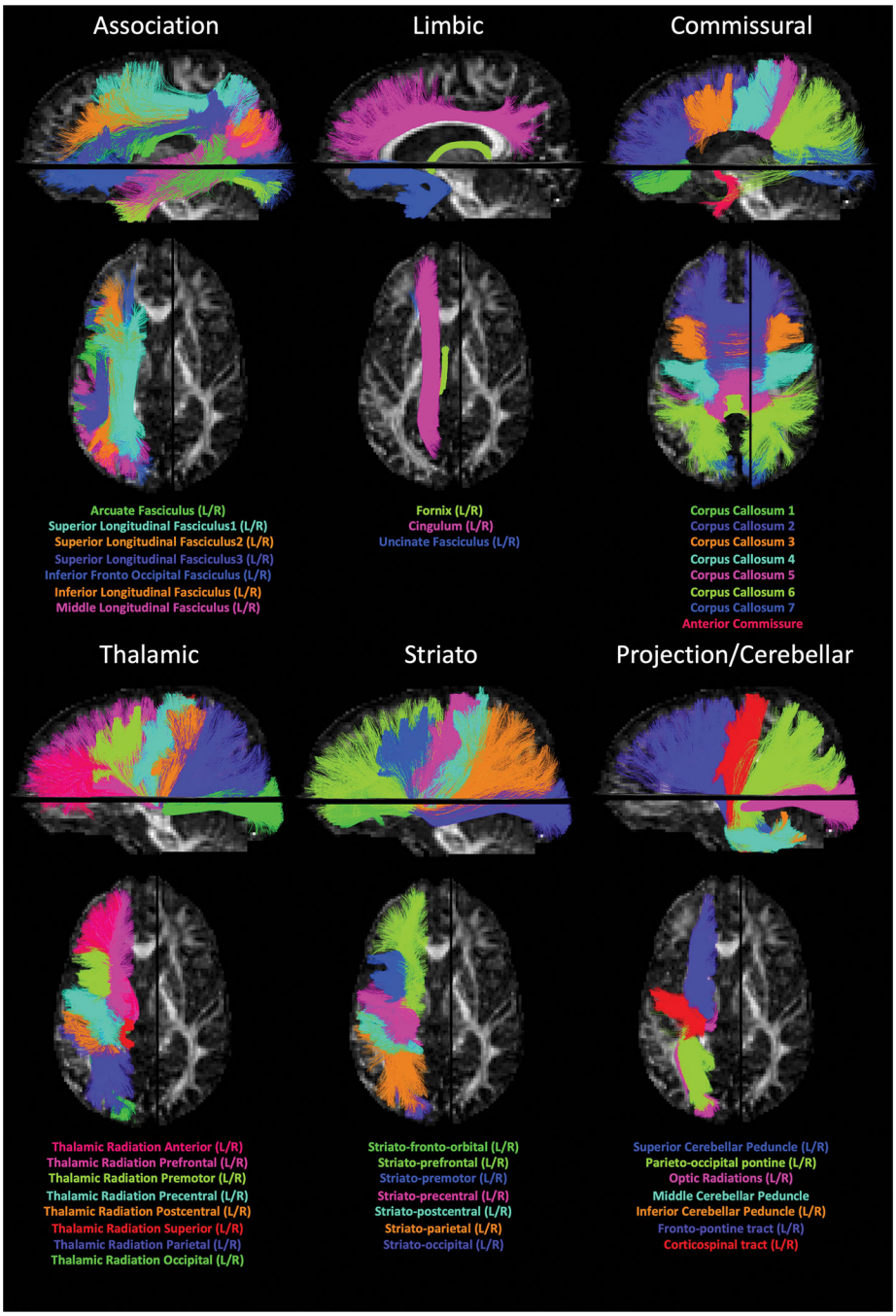

Fig. 1.

We investigated microstructure and macrostructure features of 71 pathways virtually dissected using TractSeg (Wasserthal et al. 2018), visualized and organized into association, limbic, commissural, thalamic, striatal, and projection and cerebellar pathways

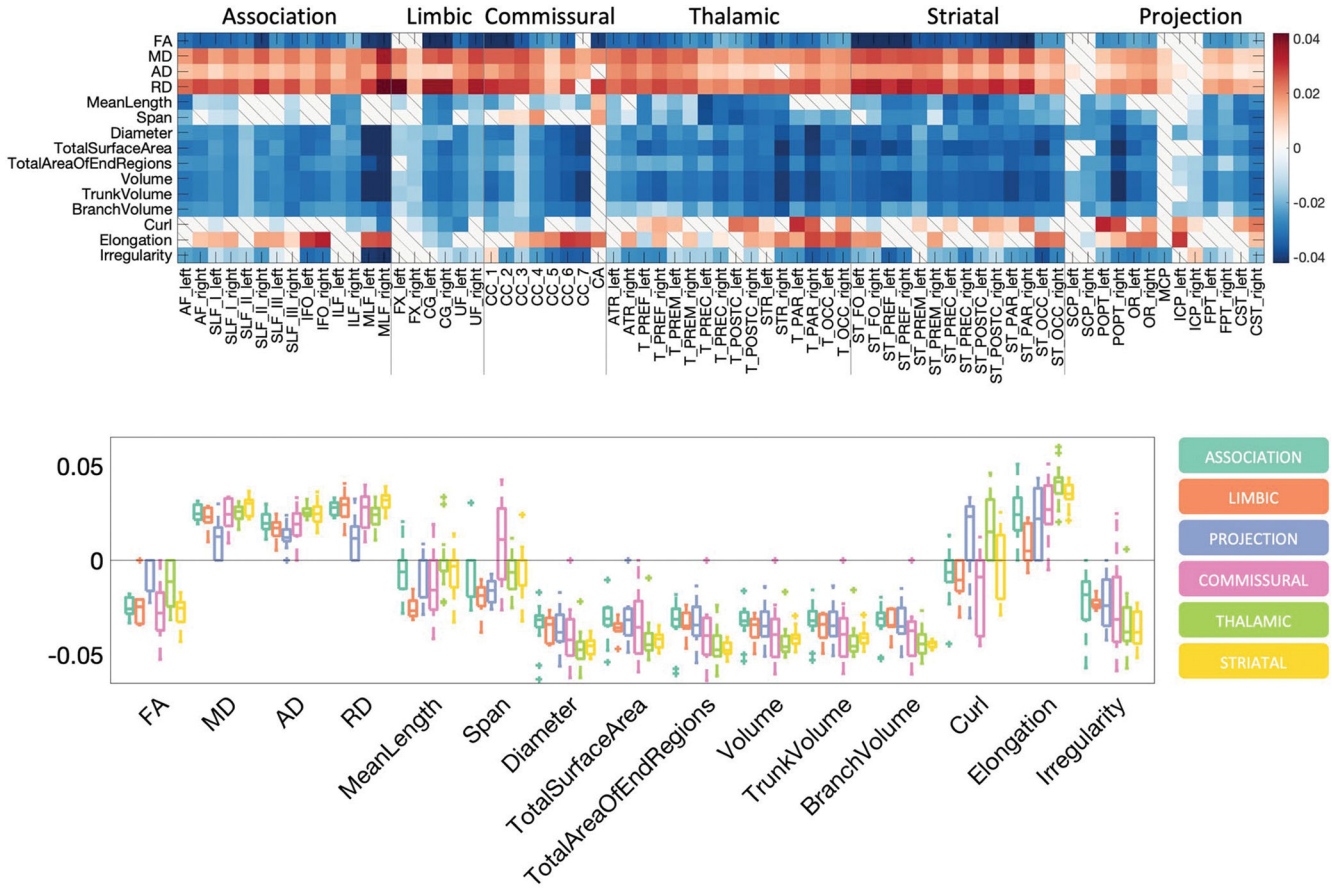

Fig. 2.

What and where changes occur during aging. The beta coefficient from linear mixed effects modeling is shown as a matrix for all features across all pathways, and also shown as boxplots for both microstructural features (left) and macrostructural features (right). Boxplots are shown separated by pathway types. Results are shown for TractSeg-derived pathways

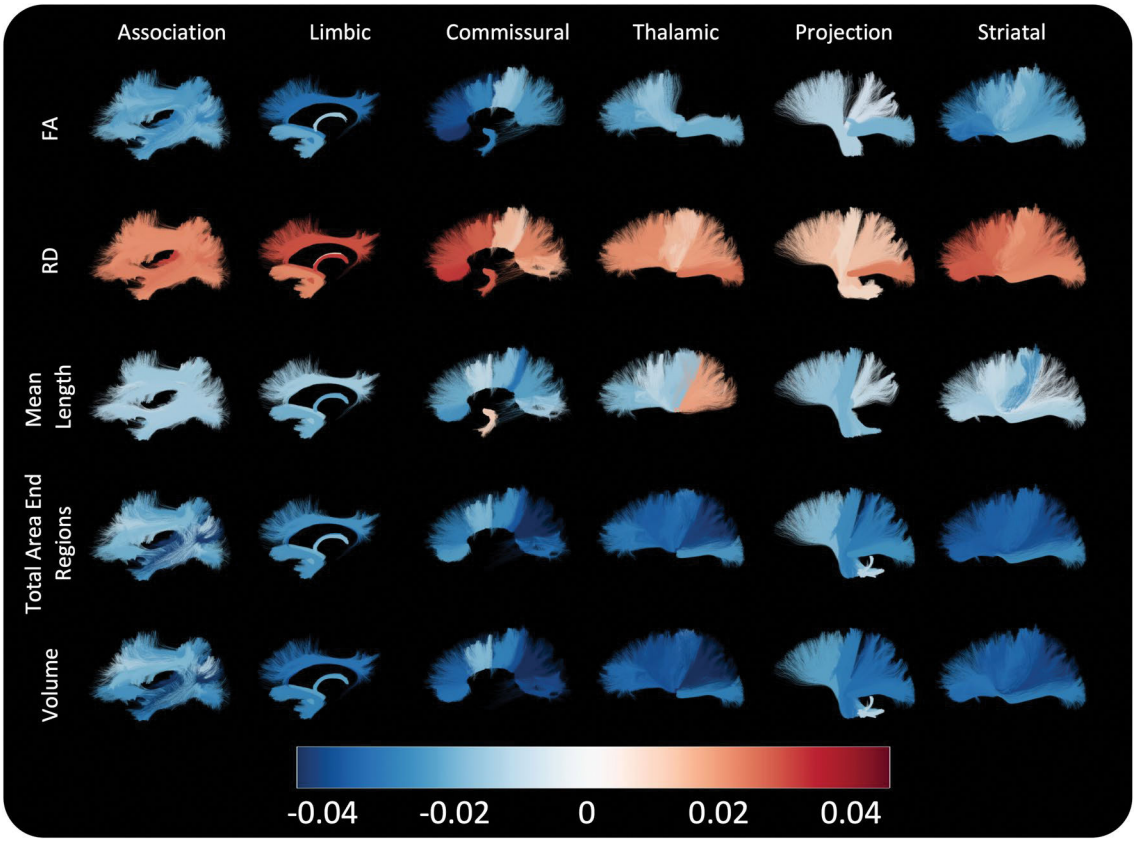

Fig. 3.

Bundle-based visualization of associations with age. Bundles that have significant associations with age are colored based on Beta-association coefficient from linear mixed-effects models, for 5 selected features. Only those with statistically significant change with age are displayed. Results are shown for TractSeg-derived pathways

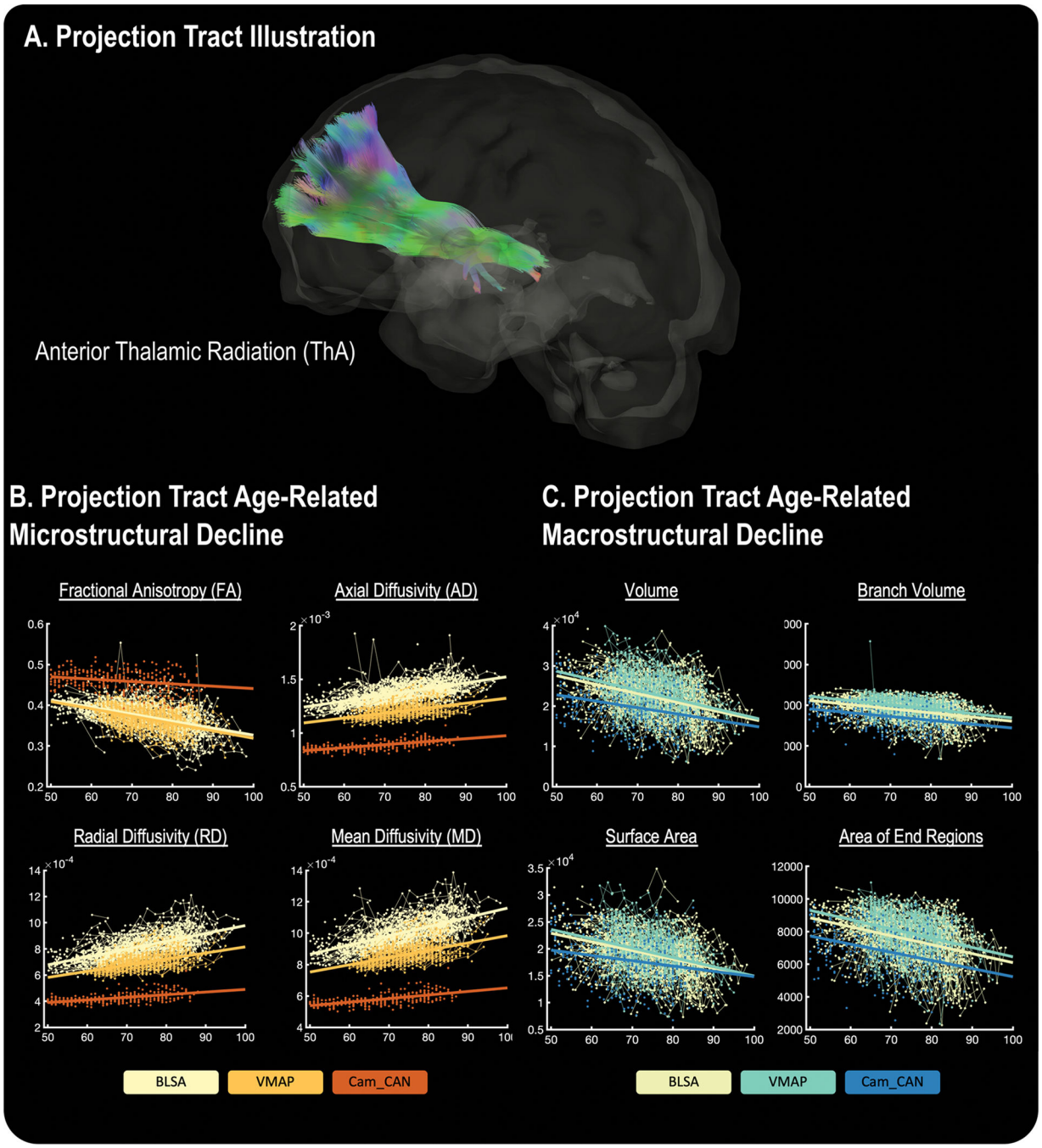

Fig. 4.

Example microstructural and macrostructural associations for a projection white matter tract. A 3D illustration of the anterior thalamic radiation (ThA) is shown (**A**), as it exhibited significant microstructural (**B**) and microstructural decline (**C**). For each microstructural and macrostructural plot, colored datapoints and lines represent individual cohorts

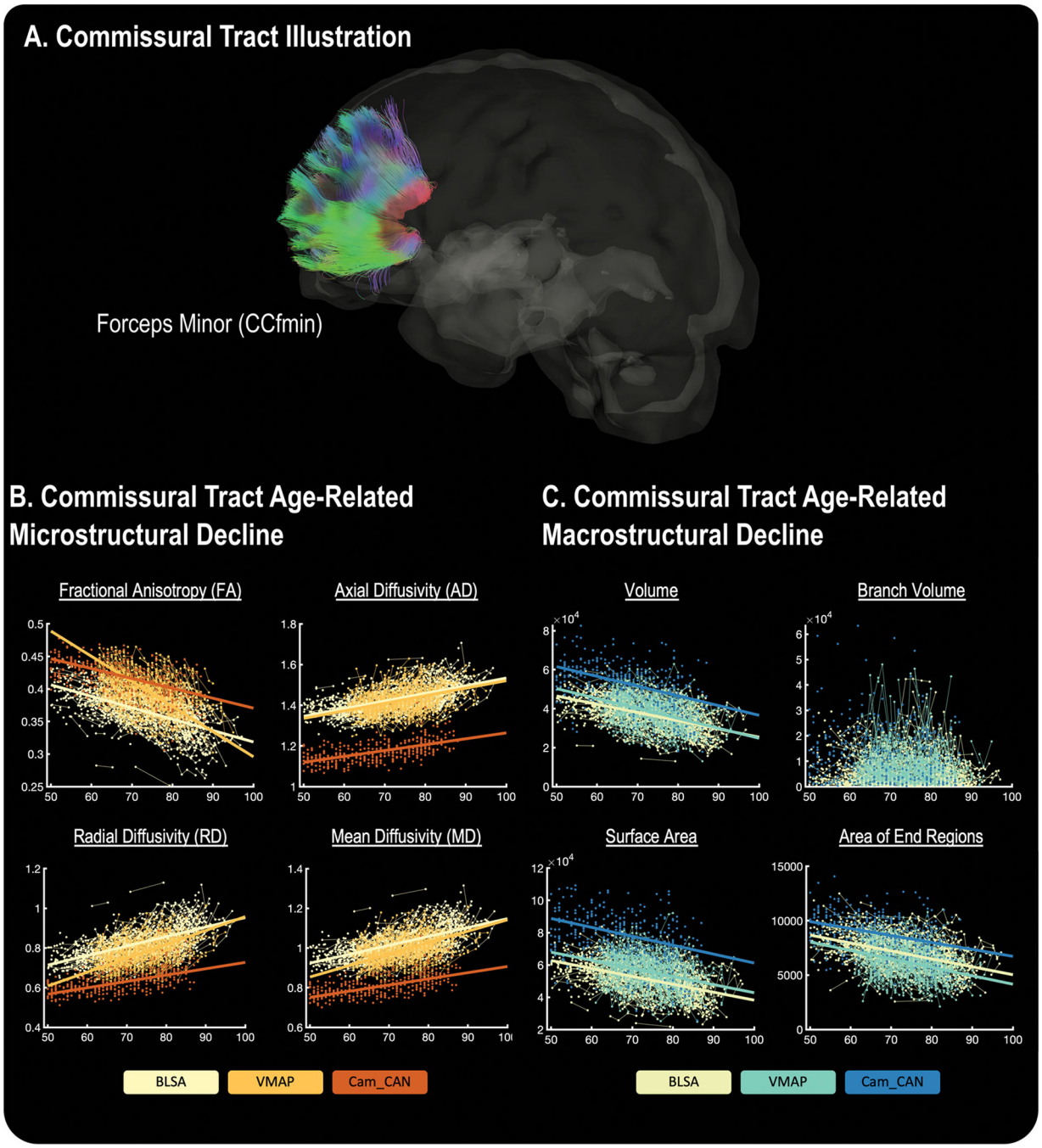

Fig. 5.

Example microstructural and macrostructural associations for a commissural white matter tract. A 3D illustration of the forceps minor (CCfmin) is shown (**A**), as it exhibited significant microstructural (**B**) and microstructural decline (**C**). For each microstructural and macrostructural plot, colored datapoints and lines represent individual cohorts

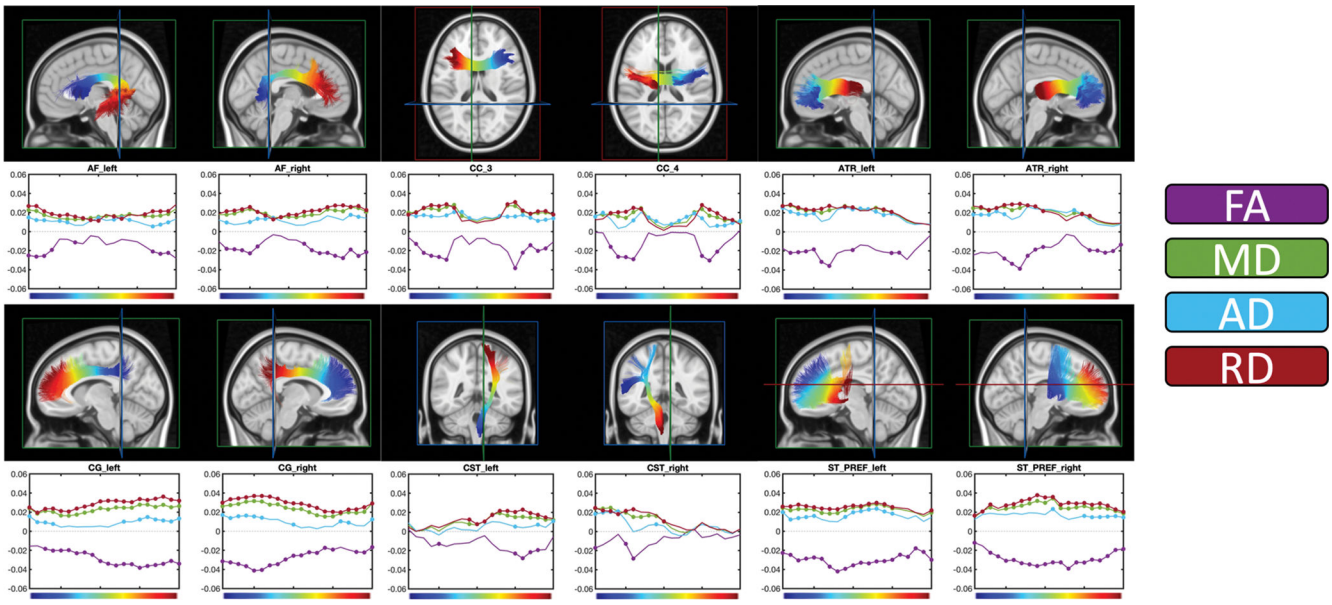

Fig. 6.

Along-tract analysis for example association, commissural, thalamic, limbic, projection, and striatal pathways. Streamlines are color coded red-to-blue based on position along pathway, while plots show beta coefficient from linear mixed modelling for FA, MD, AD, and RD. Following the bundle analytics framework (Chandio et al. 2020), positions that show significant age-related effects at a significance level of $p < 0.001$ are marked with circles

Table 1

This study used 3 longitudinal and cross-sectional data sets, with a total of 1184 subjects and 2236 sessions of healthy subjects aged 50–97 years

Dataset	Number of subjects	Number of sessions	Age
Baltimore longitudinal study of aging	675	1545	[50–97]
	290 M	Range [1–8]	73.3 (9.8)
Cambridge centre for ageing neuroscience	356	356	[50–88]
	179 M	Range [1]	67.9 (10.3
Vanderbilt memory and aging project	187	558	[60–95]
	572 M	Range [1–8]	74.2 (7.0)
	1218	**2459**	[**50–97**]
	582 M	**Range** [**1–8**]	**72.6** (**9.5**)

Brain Struct Funct. Author manuscript; available in PMC 2022 November 10.

Table 2

Macrostructural features, and their definitions

Feature	Units	Type	Equation	Definition
Length	mm	Length	$\frac{1}{n}\sum_{i=1}^{i=n}\sum_{t=1}^{t=m_i-1}\|v_i(t)-v_i(t+1)\|_2$	Length of bundle trajectory
Span	mm	Length	$\frac{1}{n}\sum_{i=1}^{i=n}\|v_i(1)-v_i(m_i)\|_2$	Distance between two ends of the bundle
Diameter	mm	Length	$2\sqrt{\frac{\text{volume}}{\pi\times\text{length}}}$	Average bundle diameter (when approximated using cylinder model)
Radius of End Regions	mm	Length	$\frac{1.5}{N_e}\sum_{i=1}^{i=N_e}\|E_i-\bar{E}_i\|_2$	Coverage of end areas (when approximated using circular model)
Surface Area	mm^2	Area	$N_s\times\text{voxelspacing}^2$	Total surface area of bundle
Area of End Regions	mm^2	Area	$N_e\times\text{voxel spacing}^2$	Total surface area of both end regions
Volume	mm^3	Volume	$N\times\text{voxel volume}$	Total tract volume
Trunk Volume	mm^3	Volume	$N_t\times\text{voxelvolume}$	Portion of bundle connecting the two largest components of the end regions
Branch Volume	mm^3	Volume	$N_b\times\text{voxel volume}$	Portion of bundle connecting areas that 'branch' from largest end region
Curl	N/A	Shape	$\frac{\text{Length}}{\text{Span}}$	Range from 1 to infinity, with larger curl indicating greater curvature
Elongation	N/A	Shape	$\frac{\text{Length}}{\text{Diameter}}$	Ratio of length to diameter
Irregularity	N/A	Shape	$\frac{\text{Surfacearea}}{\pi\times\text{Diameter}\times\text{Length}}$	Irregularity based on cylinder model (surface area larger than expected cylinder surface suggests higher irregularity)

See (Yeh 2020) for complete descriptions and justifications

Following (Yeh 2020), a fiber bundle is a set of streamline trajectories that is represented as 3D coordinate sequences: vi(*t*) | *i* = 1, 2, 3,...n, where *n* is the total number of tracks, vi(*t*) is a sequence of 3D coordinates representing the trajectory of a track. *t* is a discrete variable from 1 to mi, where mi is the number of the coordinates

Bundle: trajectory form= {vi(t) | i = 1, 2, 3, ...n}, voxelized form={V |i = 1, 2, 3,...N}

End surface: voxelized form= $\{E_i=1,2,3,...N_e\}$, where E_i are voxel coordinates

N_t is the number of "trunk bundle" voxels

N_s is the number of tract surface voxels